# GENERALIZED MODELING OF MILLING MECHANICS AND DYNAMICS: PART II - INSERTED CUTTERS

**Serafettin Engin**
Graduate Student
<engin@mech.ubc.ca>

**Yusuf Altintas**
Professor and ASME Fellow
<altintas@mech.ubc.ca>

The University of British Columbia
Department of Mechanical Engineering
2324 Main Mall, Vanocuver, B.C. , V6T 1Z4, CANADA
tel: (604) 822 21 82, fax: (604) 822 24 03

## ABSTRACT

Inserted cutters are widely used in roughing and finishing of parts. The insert geometry and distribution of inserts on the cutter body vary significantly in industry depending on the application. This paper presents a generalized mathematical model of inserted cutters for the purpose of predicting cutting forces, vibrations, dimensional surface finish and stability lobes in milling. In this paper, the edge geometry is defined in the local coordinate system of each insert, and placed and oriented on the cutter body using cutter's global coordinate system. The cutting edge locations are defined mathematically, and used in predicting the chip thickness distribution along the cutting zone. Each insert may have a different geometry, such as rectangular, convex triangular or a mathematically definable edge. Each insert can be placed on the cutter body mathematically by providing the coordinates of insert center with respect to the cutter body center. The inserts can be oriented by rotating them around the cutter body, thus each insert may be assigned to have different lead and axial rake angles. By solving the mechanics and dynamics of cutting at each edge point, and integrating them over the contact zone, it is shown that the milling process can be predicted for any inserted cutter. A sample of inserted cutter modeling and analysis examples are provided with experimental verifications.

## NOMENCLATURE:

| | | |
|---|---|---|
| X, Y, Z | : | Cutter coordinate system |
| $O$ , $O'$ | : | Cutter and insert center points |
| $a$ , $b$ | : | Rectangular insert width and height |
| $h(\phi, z)$ | : | Instantaneous chip thickness |
| u, v, w | : | Insert local coordinate system |
| $\beta$ , $\delta$ , $\varphi$ | : | Insert rotation angle around X, Y, Z axes |
| $T_M$ | : | Total transformation matrix for the insert |
| $R, \theta_s, \theta_e, o_f$ | : | Convex triangular insert dimensions |
| $dF_t$, $dF_r$, $dF_a$ | : | Differential tangential, radial and axial force components acting on a chip element, respectively |
| $K_{tc}$ , $K_{rc}$ , $K_{ac}$ | : | Cutting force coefficients in tangential, radial and axial directions, respectively |
| $K_{te}$ , $K_{re}$ , $K_{ae}$ | : | Cutting coefficients in tangential, radial and axial directions, respectively |
| $F_x$ , $F_y$ , $F_z$ | : | Cutting forces in X, Y, Z directions, respectively |
| $I_r$ , $I_z$ | : | Insert center radial and axial distance from cutter tip, respectively |
| $\vec{V}_{IC}$ | : | Insert center position vector from cutter center |
| $\vec{V}_{CE}$ | : | Cutting edge position vector from insert center |
| $\vec{V}_{CER}$ | : | Cutting edge position vector from insert center after rotations |
| $\vec{V}_p$ | : | Cutting edge position vector from cutter center |
| $R_x(\beta), R_y(\delta), R_z(\varphi)$ | : | Insert rotation matrixes for X, Y, Z, respectively |

## 1. INTRODUCTION

Inserted face and end milling cutters are widely used in industry. Face milling cutters have evenly or unevenly spaced inserts, and used in removing excess material from the face of parts such as transmission box, engine block or machine tool columns and beds. Inserts are distributed in both radial and axial directions on indexed end mills. Indexed cutters are used in removing massive amount of material from the periphery of parts such as aircraft spars, airframe support structures and rough pocketing of dies and molds. The distribution of inserts may be regular or arbitrary depending on the application. In order to improve the surface finish, chatter stability and cutting force balancing on the cutter body, the inserts with various shapes can be placed on the milling cutter body.

The industry requires a generalized mathematical model, which allows the analysis of all inserted milling cutters used in practice (Wertheim *et al.*, 1994). However, the research in the past mainly focused on the modeling of mechanics and dynamics of special cutter geometry. Fu *et al.* (1984) provided a comprehensive modeling of

inserted face milling cutters. They modeled rectangular inserts with corner radius, and introduced equivalent lead and rake angles, which are related to experimentally identified cutting constants. Fu *et al.*'s work (1984) became a basis for a number of successive mechanistic models in milling, and lead to the improved static and dynamic modeling of milling (Kim and Ehman, 1993). The mechanistic approach allowed to the integration of milling mechanics and to the optimization of cutting conditions during tool path planning on CAD/CAM systems dynamics (Gu *et al.*, 1997; Spence *et al.*, 1994). The cutting forces are assumed to be proportional to the instantaneous chip area in most face milling cases, but the variation of cutting pressure along the curved cutting edge is also considered in some of the more rigorous models (Endres *et al.*, 1995). Spieawak (1994) presented an analytical methods in integrating the spindle tilt, runout and eccentricity in identifying the chip thickness. However, a generalized handling of mechanics and dynamics of inserted end mills have not received similar attention. Majority of the research up to now focused on the accurate identification of chip load in static and dynamic milling and identification of cutting constants for a single insert.

This paper presents a generalized modeling of cutting force system in the inserted cutters. The cutting edge is defined mathematically in a local coordinate system of each insert. Each insert may have a different geometry, such as rectangular, convex triangular or a mathematically definable edge. Each insert can be placed on the cutter body mathematically by providing the coordinates of insert center with respect to the cutter body center. The inserts can be oriented by rotating them around the cutter body, thus each insert may be assigned to have different lead and axial rake angles. The cutting edge geometry of each insert on the cutter is mathematically expressed. The cutter is divided into small disk elements, and the mechanics and dynamics of milling can be solved for each cutting edge element. The literature provides various approaches in determining the cutting constant and dynamic chip load as a function of local cutting edge geometry. The reported process modeling techniques, which are not repeated but only cited here, are used along the cutting edge. By integrating the structural dynamics of workpiece and cutter into the mathematical model, the performance of a general indexed cutter can be simulated. The generalized model allows prediction of cutting forces, dimensional surface finish, chatter and forced vibrations, and chatter stability lobes for a variety of inserted face and helical end mills. The paper provides milling examples for two different inserted end mills.

Henceforth, the paper is organized as follows. The geometric modeling of inserted cutters is provided in Section 2. The mechanics and dynamics of milling used in this particular work are summarized in Section 3, and the details of the process models are cited to the relevant literature. Prediction of cutting forces, vibrations, dimensional surface finish, and chatter stability was demonstrated using two different inserted helical end mils. The simulation and experimental results are given in Section 4, and the paper is concluded with the summary of contributions in Section 5.

## 2. GENERALIZED GEOMETRIC MODEL OF INSERTED CUTTERS

The purpose of the geometric model is to predict the mechanics and dynamics of cutters with arbitrary insert shapes and distribution. First, the mathematical model of one insert placed on a cutter body and then the definition of a general cutter with varying inserts along its periphery are presented.

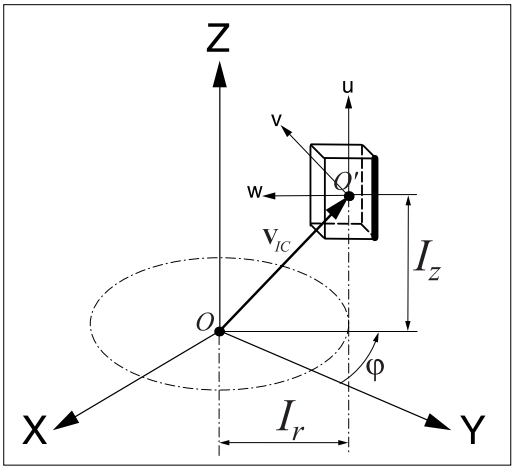


**Figure 1.** Location vector of insert center on the cutter.

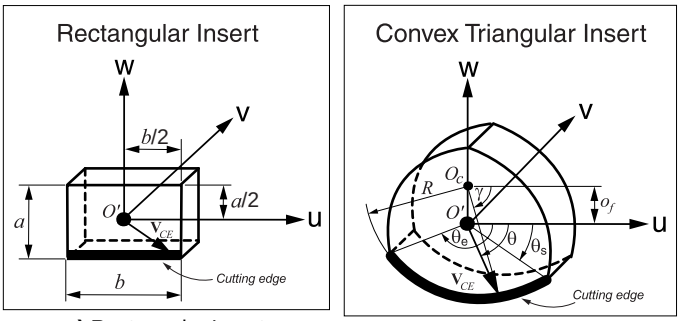


**a)** Rectangular Insert **b)** Convex triangular insert

**Figure 2.** Geometry of inserts.

**Mathematical Model of Insert:** The cutter body is defined in Cartesian coordinate system (XYZ), and the center of the insert is aligned with a second coordinate system (uvw), see Figure 1. A vector between the cutter tip and insert centers is,

$$\vec{V}_{IC} = -\sin\varphi\ I_r\ \vec{i} + \cos\varphi\ I_r\ \vec{j} + I_z\ \vec{k} \qquad (1)$$

where $I_r$ is the radial offset in XY plane, $I_z$ is the axial offset of the insert center from the cutter axis (Figure 1). The face of the insert where the cutting edge lies, is aligned with the uw plane of the insert coordinate system (i.e. $v$=0). The insert center is indexed by an angular distance of $\varphi$ measured counter-clockwise from the Y axis, see Figure 1. The insert is placed on the cutter body using the vector defined in Eq. (1).

The insert shapes can vary depending on the application and manufacturer. Two most commonly insert shapes are considered to illustrate the generalized modeling approach, see Figure 2. The rectangular insert is defined by the cutting edge length ($b$) and insert width ($a$). The convex triangular insert is defined by the radius ($R$) of curved cutting edge, offset ($o_f$) between the insert center ($O'$) and cutting edge curvature center ($O_c$), and by the angular boundaries ($\theta_s, \theta_e$) of the cutting edge measured on (uw) plane in clockwise direction from local axis (u). The points along the cutting edge of the insert is defined by the vector $\vec{V}_{CE}$ in coordinate system (uvw),

$$\vec{V}_{CE} = u\,\vec{i} + v\,\vec{j} + w\,\vec{k} \qquad (2)$$

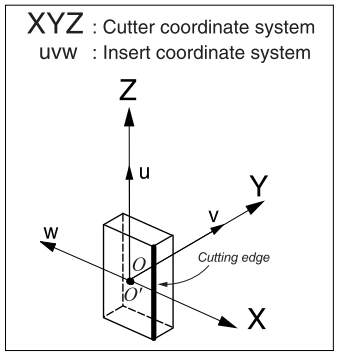


**a)** Cutter (XYZ) and insert(uvw) coordinates

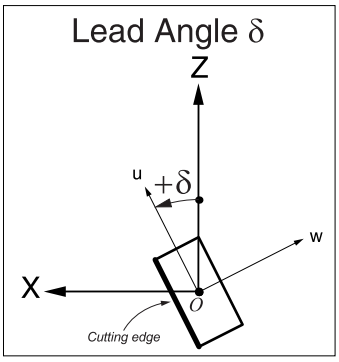


**b)** Rotation about Y axis with $\delta$ lead angle

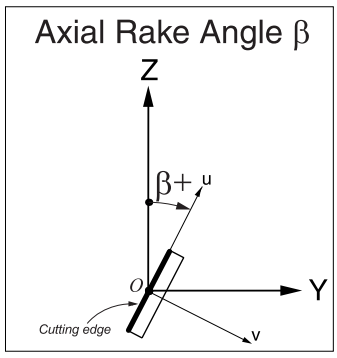


**c)** Rotation about X axis with $\beta$ axial rake angle

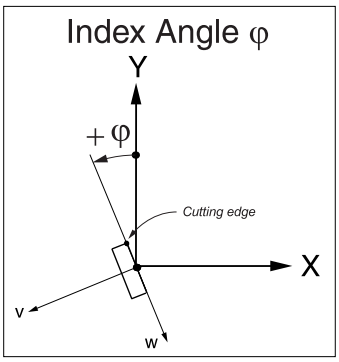


**d)** Rotation about Z axis with $\varphi$ index angle

**Figure 3.** The insert rotations.

where

$$-\frac{b}{2} \le u \le \frac{b}{2}; \quad v = 0; \quad w = \frac{a}{2} \qquad \text{for rectangular insert}$$

$$\left.\begin{aligned} u &= R\cos\gamma; \quad v = 0; \quad w = -R\cos\gamma + o_f \\ \gamma &= \theta + \sin^{-1}\left(\frac{o_f}{R}\cos\theta\right) \text{ for } \theta_s \le \theta \le \theta_e \end{aligned}\right\} \quad \text{for convex triangular inserts}$$

Note that (uvw) plane of the insert's coordinate system is aligned with the insert face, which contains the cutting edge (i.e. $v$=0). The insert's cutting edge is defined locally in insert coordinate system (uvw).

Each insert can be oriented on the cutter body by rotating it around the global cutter body axis X, Y and Z (Figure 3). The insert is rotated at amount of *lead angle* ( $\delta$ ) about axis (Y), *axial rake angle* ( $\beta$ ) about axis (X), and *index angle* ( $\varphi$ ) about axis (Z). The corresponding rotation matrixes for X, Y and Z are as follows, respectively.

$$\left.\begin{aligned} \mathrm{R}_x(\beta) &= \begin{bmatrix} 1 & 0 & 0 \\ 0 & \cos\beta & \sin\beta \\ 0 & -\sin\beta & \cos\beta \end{bmatrix}; \quad \mathrm{R}_y(\delta) = \begin{bmatrix} \sin\delta & 0 & -\cos\delta \\ 0 & 1 & 0 \\ \cos\delta & 0 & \sin\delta \end{bmatrix}; \\ \mathrm{R}_z(\varphi) &= \begin{bmatrix} -\sin\varphi & -\cos\varphi & 0 \\ \cos\varphi & -\sin\varphi & 0 \\ 0 & 0 & 1 \end{bmatrix} \end{aligned}\right\} \quad (3)$$

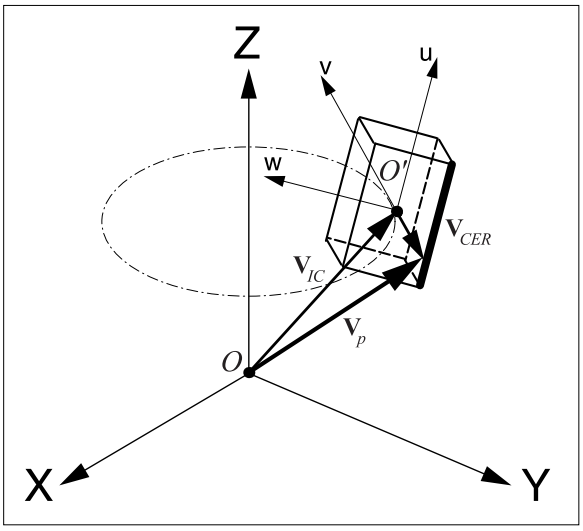


**Figure 4.** The cutting edge position vector.

If the insert is rotated about all three axis, the resulting transformation matrix is,

$$\mathrm{T}_M = \mathrm{R}_z(\varphi)\cdot\mathrm{R}_x(\beta)\cdot\mathrm{R}_y(\delta) = \begin{bmatrix} -\sin\varphi\sin\delta - \cos\varphi\sin\beta\cos\delta & -\cos\varphi\cos\beta & \sin\varphi\cos\delta - \cos\varphi\sin\beta\sin\delta \\ \cos\varphi\sin\delta - \sin\varphi\sin\beta\cos\delta & -\sin\varphi\cos\beta & -\cos\varphi\cos\delta - \sin\varphi\sin\beta\sin\delta \\ \cos\beta\cos\delta & -\sin\beta & \cos\beta\sin\delta \end{bmatrix} \quad (4)$$

The coordinates of the cutting edge in insert coordinate system becomes (Figure 4):

$$\mathrm{V}_{CER} = \mathrm{T}_M \cdot \mathrm{V}_{CE} = [\mathrm{T}_M]\begin{bmatrix} u \\ v \\ w \end{bmatrix} \quad (5)$$

The final position of the cutting edge with respect to cutter body coordinate system becomes,

$$\vec{\mathrm{V}}_p = \vec{\mathrm{V}}_{IC} + \vec{\mathrm{V}}_{CER} = -\sin\varphi\, I_r\, \vec{\mathrm{i}} + \cos\varphi\, I_r\, \vec{\mathrm{j}} + I_z\, \vec{\mathrm{k}} + [\mathrm{T}_M]\begin{bmatrix} u \\ v \\ w \end{bmatrix} =$$

$$\begin{aligned} &\left[-\sin\varphi(u\sin\delta - w\cos\delta + I_r) - \cos\varphi\sin\beta(u\cos\delta + w\sin\delta) - v\cos\varphi\cos\beta\right]\vec{\mathrm{i}} \\ &+\left[\cos\varphi(u\sin\delta - w\cos\delta + I_r) - \sin\varphi\sin\beta(u\cos\delta + w\sin\delta) - v\sin\varphi\cos\beta\right]\vec{\mathrm{j}} \\ &+\left[\cos\beta(u\cos\delta + w\sin\delta) - v\sin\beta + I_z\right]\vec{\mathrm{k}} \end{aligned} \quad (6)$$

Once the insert center location $(I_r, I_z)$, orientation on the cutter body $(\delta, \beta, \varphi)$, and edge dimensions $(a, b; R, \theta_s, \theta_e)$ are specified, a point on the cutting edge can be evaluated for a given elevation or axial depth of cut position $(z)$ from Eq. (6).

**Mathematical Model of Multiple Inserts:** There are various inserted cutters used in industry depending on machining applications. There may be identical inserts placed on the periphery of the cutter with equal pitch spacing (i.e. face milling cutters), helical flutes where each flute may contain multiple inserts, or randomly distributed inserts with different shapes and at different locations both in radial and axial directions. A generalized cutter design matrix $\left(D_{M\ (6\times N)}\right)$ is used in defining a cutter with a general insert distribution,

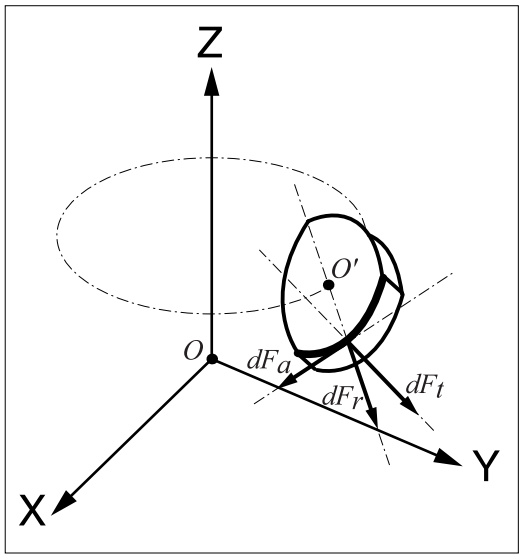


**Figure 5.** Three-dimensional cutting edge profile on the insert and cutting force directions.

$$D_M = \left[\begin{array}{cccccccc} t_{11} & t_{12} & t_{13} & \ldots; & t_{21} & t_{22} & \ldots; & \ldots \\ I_{z11} & I_{z12} & I_{z13} & \ldots; & I_{z21} & I_{z22} & \ldots; & \ldots \\ I_{r11} & I_{r12} & I_{r13} & \ldots; & I_{r21} & I_{r22} & \ldots; & \ldots \\ \delta_{11} & \delta_{12} & \delta_{13} & \ldots; & \delta_{21} & \delta_{22} & \ldots; & \ldots \\ \beta_{11} & \beta_{12} & \beta_{13} & \ldots; & \beta_{21} & \beta_{22} & \ldots; & \ldots \\ \underbrace{\varphi_{11}}_{1.insert} & \underbrace{\varphi_{12}}_{2.insert} & \underbrace{\varphi_{13}}_{3.insert} & \underbrace{\ldots;}_{\ldots} & \underbrace{\varphi_{21}}_{1.insert} & \underbrace{\varphi_{22}}_{2.insert} & \underbrace{\ldots;}_{\ldots} & \underbrace{\ldots}_{\ldots} \\ & & & \underbrace{\qquad\qquad}_{1.\,flute} & & & \underbrace{\qquad\qquad}_{2.\,flute} & \underbrace{\qquad}_{\ldots} \end{array}\right] \quad (7)$$

where $N$ is the number of inserts on the cutter. The first and the second digits of subindices represent flute number and insert order number from tool tip, respectively. Note that it is not necessary to have equal number of inserts on each flute. Each column represents one insert with its type and position on the cutter body. The first element $(t)$ of each column represents the insert type, i.e. $t = 0$ : no insert, $t = 1 \ldots 10$: rectangular insert family, $t = 11...20$ triangular insert family. The remaining five parameters define the position and orientation of the insert on the cutter body. Rectangular inserts have two parameters that are width ($a$) and length ($b$) (Figure 2a). The convex triangular insert has four parameters that are the starting angle ( $\theta_s$ ) and the end angle ( $\theta_e$ ), radius of arc ($R$) and the arc radius center offset from the center of insert ( $o_f$ ) (Figure 2b). Each insert shape is separately stored in a database with its associated dimensions.

## 3. MODELING OF CUTTING FORCES

Consider differential cutting forces ( $dF_t$, $dF_r$, $dF_a$ ) are produced when cutting an infinitesimal chip element which has a local uncut chip thickness of $h(\phi, z)$ normal to the cutting edge, chip height of $dz$ and curved edge contact length of $dS$ (Figure 5).

$$\left.\begin{array}{rcl} dF_t &=& K_{te}(z)\ dS + K_{tc}(z)\ h(\phi,z)\ dz \\ dF_r &=& K_{re}(z)\ dS + K_{rc}(z)\ h(\phi,z)\ dz \\ dF_a &=& K_{ae}(z)\ dS + K_{ac}(z)\ h(\phi,z)\ dz \end{array}\right\} \quad (8)$$

The edge force cutting coefficients, $K_{te}$, $K_{re}$, $K_{ae}$ represent the non-shearing flank line contact forces, and the force coefficients $K_{tc}$, $K_{rc}$, $K_{ac}$ represent shear or rake face contact pressure. The linearized force model used in Eq. (8) is presented in detail by Budak *et al.* (1996). It should be noted that the inserts used in industry may have varying rake face and curvature along its cutting edge. For example, chip breaking grooves and non-uniform rake face may exist on each insert. The cutting coefficients can be identified from orthogonal cutting parameters (average shear stress, shear angle and friction coefficient) by transforming them into oblique cutting domain (Budak *et al.*, 1996), if the rake face is uniform like in regular end mills. However, if the insert's cutting edge has a chamfer or radius, and the rake face of the insert is non-uniform, orthogonal to oblique cutting transformation may not lead to an accurate evaluation of cutting coefficients (Endres *et al.* 1995). Depending on the insert shape and cutting edge geometry, it may be more appropriate to use mechanistic models in identifying the cutting coefficients as a function of edge position $(z)$, cutting speed, local chip thickness. The mechanistic approaches for the identification of cutting constants are well presented in literature (Fu *et al.*, 1984; Gu *et al.*, 1997; Endres *et al.* 1995; Kim and Ehmann, 1993). The evaluation of chip thickness with and without chatter vibrations have been presented in detail by Altintas and Lee (1998). The details of mechanistic identification of cutting constants and milling process modeling can be found in the cited literature, and are used but not repeated here (Ehmann *et al.*, 1997). The cutter is divided into small axial disk elements with a differential height of *dz*. The uncut chip thickness removed by each differential segment along the insert is identified by considering the trochoidal motion of the milling (Martelotti, 1945) and the regenerative chatter vibration of both cutter and workpiece (Montgomery and Altintas, 1991). If the insert has roundness, the chip thinning is considered using a similar method used in ball end milling (Altintas and Lee, 1998). The differential cutting forces are evaluated and transformed into Cartesian coordinates of the cutter similar to the method used for helical end mills, see Part I of the paper (Engin and Altintas, 1999). The differential forces are summed along all inserts, which are in contact with the workpiece. The resulting cutting forces in the three directions are applied to the structural dynamic models of cutter and workpiece (Montgomery and Altintas, 1991) to evaluate the structural displacements and their influence on the regenerative chip thickness. The dynamic chip thickness ( $h(\phi, z)$ ) is evaluated at small time intervals by rotating the cutter and feeding the workpiece. The time domain simulation model allows predictions of dynamic chip thickness, cutting forces, vibrations of both cutter and workpiece along the depth of cut, surface finish and chatter stability lobes (Altintas and Lee, 1998; Altintas *et al.* 1992). The chatter stability lobes for the inserted cutters are also identified in frequency domain using the analytical solution proposed by Altintas and Budak (1995). The cited models of milling process mechanics, kinematics, dynamics and process simulations are all used here, and the readers are referred to the indicated publications for the comprehensive understanding of the models.

## 4. SIMULATION AND EXPERIMENTAL RESULTS

The proposed generalized inserted cutter model, and its corresponding mechanics and dynamics are integrated into the comprehensive milling process simulation package (MillPro, 1998). The advanced simulation program contains all the process models cited in the previous section. Two sample cases are presented here to illustrate the proposed model.

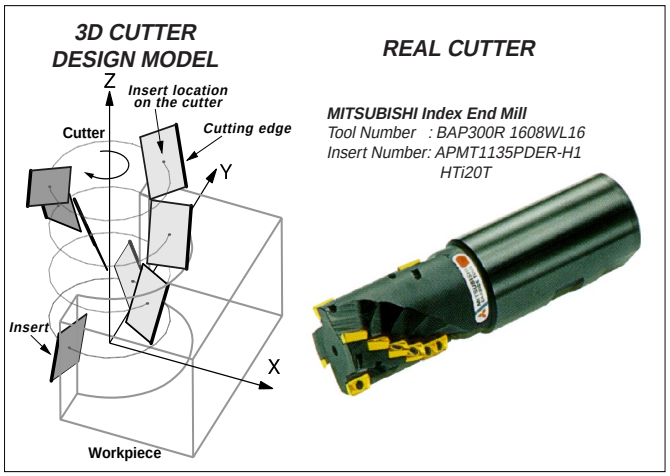


**Figure 6.** Mitsubishi inserted cutter Cutter I (Cutter number: BAP300R 1608WL16; Insert number: APMT1135PDER-H1 "insert dimensions; *a*=6.35 mm, *b*=9.8 mm" HTi20T). See Eq. (9) for insert location parameters. Shank diameter=25.4 mm, Cutter diameter=25.4 mm, 2 flutes, 4 inserts on every flute.

**Milling of AL7075 with Cutter I:** A two fluted helical inserted cutter with 25.4 mm diameter and 4 rectangular inserts on each flute is modeled (Figure 6). The cutter body is Mitsubishi BAP300R 1608WL16, with Mitsubishi APMT1135PDER-H1 HTi20T rectangular inserts (*a*=6.35 mm, *b*=9.8 mm). The design matrix of the cutter is constructed as:

$$D_M = \begin{bmatrix} 2 & 2 & 2 & 2 & ; & 2 & 2 & 2 & 2 \\ 4.6 & 13.1 & 17.7 & 22.3 & ; & 4.7 & 13.2 & 17.8 & 22.4 \\ 9.5 & 9.5 & 9.5 & 9.5 & ; & 9.5 & 9.5 & 9.5 & 9.5 \\ 0.0 & 0.0 & 0.0 & 0.0 & ; & 0.0 & 0.0 & 0.0 & 0.0 \\ 20.0 & 20.0 & 20.0 & 20.0 & ; & 10.0 & 20.0 & 20.0 & 20.0 \\ 0.0 & 40.0 & 80.0 & 120.0 & ; & 190.0 & 270.0 & 310.0 & 350.0 \end{bmatrix} \quad (9)$$

Note that the first insert of the second flute (raw 5, column 5) has an axial rake of 10 degrees, where the rest of the inserts have an axial rake of 20 degrees. The lead angles of all inserts are zero, i.e. raw 4. The cutter is used to machine Al-7075. The cutting coefficients are identified mechanistically from the measured average cutting forces per tooth period. Slot milling tests were conducted with one insert by increasing the axial depth of cut with 1.0 mm increments up to insert's edge length (Budak *et al.*, 1996). The insert's rake face geometry varies significantly along the cutting edge. Therefore the cutting coefficients are highly dependent on the axial location of the cutting edge point. The cutting coefficients are identified for each 1.0 mm segment. When the depth of cut is 5.0 mm for example, the measured average forces for 4.0 mm axial depth of cut were subtracted before identifying the cutting coefficients for the 5.0 mm edge zone. The cutting tests were conducted at a feed rate range of 0.025 to 0.200 mm/tooth at 0.025 mm/tooth increments. After identifying the cutting constants for each edge position, a satisfactory polynomial was fitted to represent them along the insert's cutting edge. The identified cutting coefficients for the two different inserts are given in Table 1. Statistical analysis result, the correlation coefficient, for each set is provided. The closeness of correlation coefficient to unity represents the improved accuracy of the curve fitting. Higher order polynomials were also used, but the improved accuracy was not sufficient to justify the complexity in expressing the cutting coefficients. The cutter is attached to a taper 40 spindle with a mechanical chuck. The transfer functions $([\Phi_{xx}(s)] = \{x\}/\{F_x\}, [\Phi_{yy}(s)] = \{y\}/\{F_y\})$ of the cutter mounted on the spindle was measured with impact hammer tests, and the identified modal parameters are given in Table 2. The transfer function model has the following structure:

$$\frac{x}{F} = [\Phi_{xx}(s)] = \sum_{k=1}^{K} \frac{[R_{1x} + R_{2x}s]_k}{s^2 + 2\zeta_{x,k}\omega_{x,k}s + \omega_{x,k}^2}$$

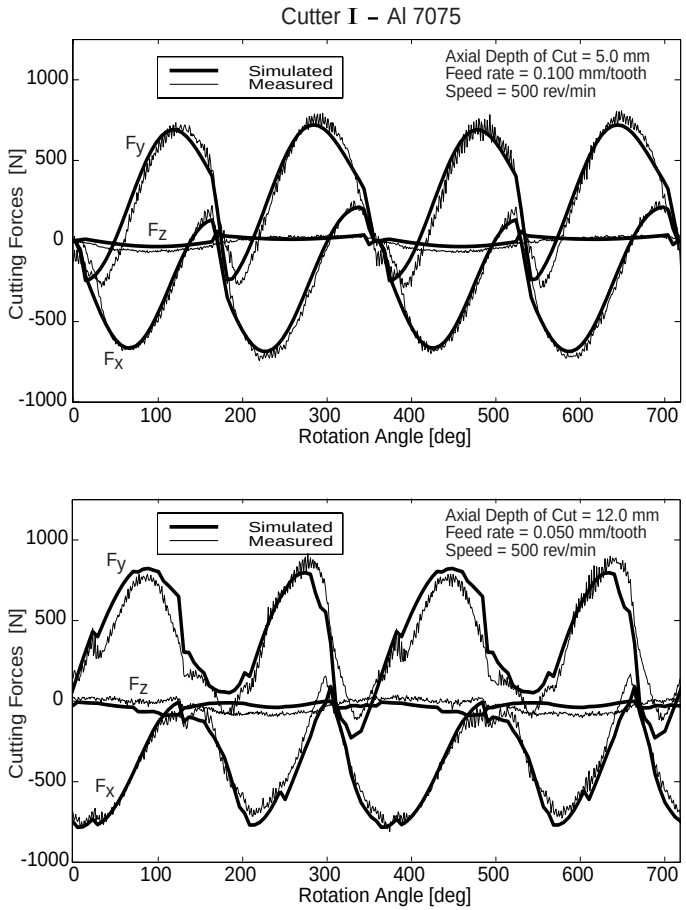


**Figure 7.** Measured and predicted cutting forces for Al-7075 with Cutter I. Cutting type is slotting. See Figure 6. for tool geometry and Table 1 for cutting coefficients.

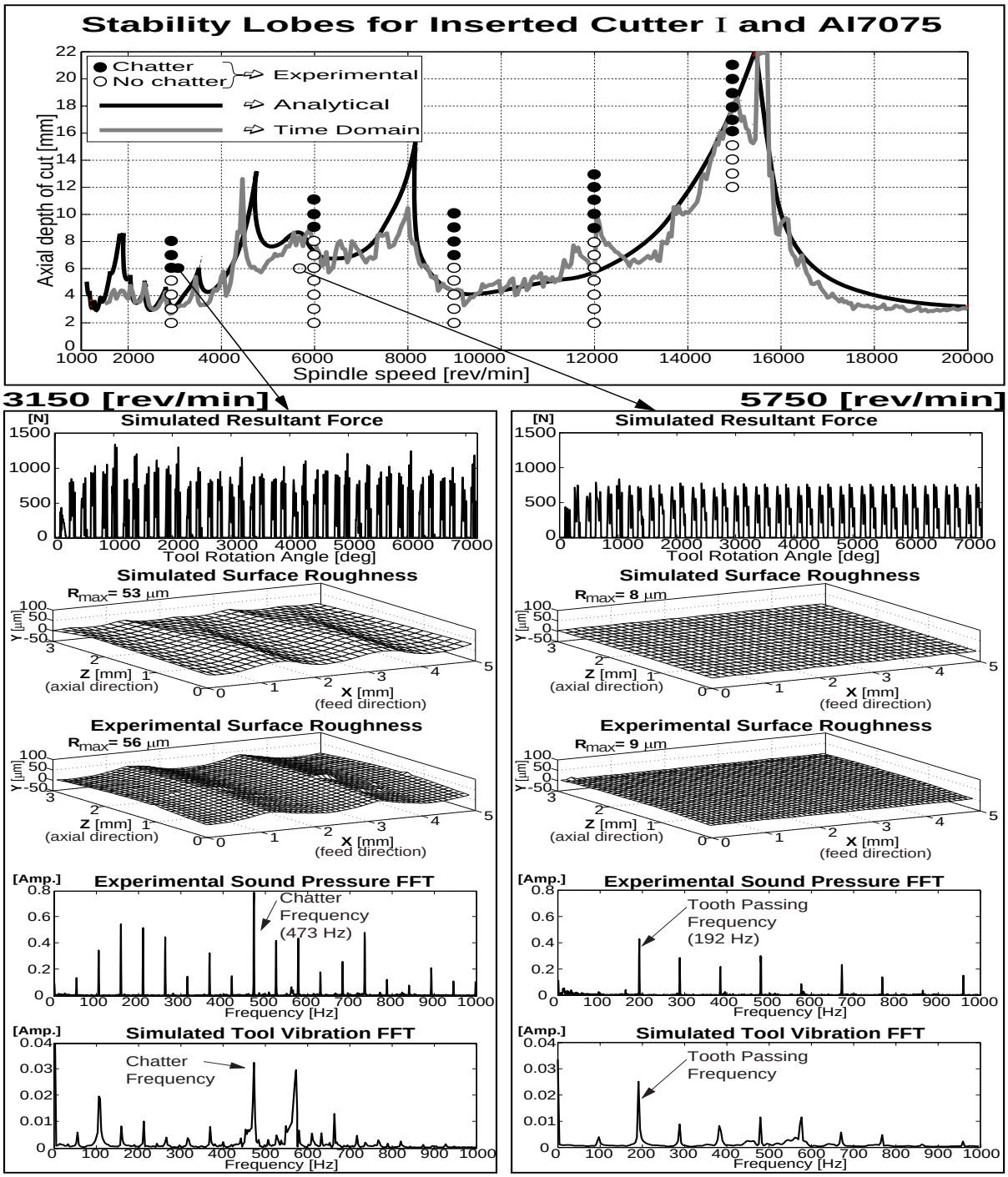


**Figure 8.** Stability lobes for Al-7075 with Cutter I (see Figure 6. ). Cutting conditions: half immersion down milling, $N_f$ =2 flutes, diameter=25.4 mm, feed rate=0.050 mm/tooth. See Table 1 for cutting coefficients Al-7075 and Table 2 for the transfer function parameters.

where $x$, $F$ are the vibration and force in the feed direction, respectively. $\varsigma_{x,k}, \omega_{x,k}$ are the damping ratio and natural frequency for mode $k$, and $K$ is the number modes. The modal parameters are evaluated from estimated complex mode residues $(\sigma_k \pm i\upsilon_k)$ as $R_{1x,k} = 2(\zeta_{x,k}\omega_{nx,k}\sigma_k - \omega_{dx,k}\upsilon_k)$, $R_{2,k} = 2\sigma_k$. Similar terminology is used in the normal direction (Y). The use of transfer functions in frequency and time domain prediction of chatter vibrations can be found in Altintas *et al.* (1995; 1998). Using the identified cutting constants, the cutting forces are predicted for slot milling of Al7075 at different depths. The predicted and measured cutting forces agreed well, as can be seen from two sample test results shown in Figure 7.

**Table 1.** The cutting coefficients for Al7075 with Cutter I ($0 \le z \le 9.8mm$). The edge contact position ($z$) is expressed in millimeter.

| | Cutting Coef. | Fitted curve | Correla. Coef. |
|---|---|---|---|
| **10° helix angle** | $K_{tc}$ [N/mm$^2$] | $7.9z^2 - 90.4z + 1073.5$ | 0.7984 |
| | $K_{rc}$ [N/mm$^2$] | $25.98z^2 - 222.3z + 795.1$ | 0.9198 |
| | $K_{ac}$ [N/mm$^2$] | $19.55z^2 - 159.4z + 294.55$ | 0.9164 |
| | $K_{te}$ [N/mm] | $-0.34z^2 - 1.91z + 38.78$ | 0.7796 |
| | $K_{re}$ [N/mm] | $-3.15z^2 + 22.98z + 23.80$ | 0.8071 |
| | $K_{ae}$ [N/mm] | $-2.66z^2 + 27.56z - 54.80$ | 0.9195 |
| **20° helix angle** | $K_{tc}$ [N/mm$^2$] | $-5.6z^2 + 22.76z + 925.4$ | 0.9003 |
| | $K_{rc}$ [N/mm$^2$] | $-13.0z^2 + 85.6z + 409.1$ | 0.9242 |
| | $K_{ac}$ [N/mm$^2$] | $-15.3z^2 + 181.9z - 227.6$ | 0.8241 |
| | $K_{te}$ [N/mm] | $-0.04z^2 - 2.04z + 33.86$ | 0.8006 |
| | $K_{re}$ [N/mm] | $-0.46z^2 + 1.38z + 53.86$ | 0.9672 |
| | $K_{ae}$ [N/mm] | $-0.25z^2 + 2.56z - 6.92$ | 0.7754 |

**Table 2.** The transfer function parameters of Cutter I.

| Direc-tion | Mode | $\omega_n$ [Hz] | $\zeta$ [%] | Mode Residue [m/N] ($\sigma_k \pm i\upsilon_k$) |
|---|---|---|---|---|
| X | 1 | 269.20 | 4.81 | $(10.097 - i\,8.760)\cdot10^{-6}$ |
| | 2 | 447.51 | 4.66 | $(25.835 - I\,105.161)\cdot10^{-6}$ |
| | 3 | 573.79 | 4.69 | $(2.976 - I\,57.900)\cdot10^{-6}$ |
| | 4 | 1837.50 | 2.94 | $(54.251 - i\,98.720)\cdot10^{-6}$ |
| | 5 | 2843.05 | 3.10 | $(108.761 - i\,29.515)\cdot10^{-6}$ |
| | 6 | 3065.05 | 1.13 | $(63.293 - i\,0.188)\cdot10^{-6}$ |
| | 7 | 4007.50 | 0.81 | $(-8.380 - i\,31.021)\cdot10^{-6}$ |
| Y | 1 | 495.47 | 3.32 | $(8.428 - i\,169.651)\cdot10^{-6}$ |
| | 2 | 1850.98 | 2.68 | $(18.614 - i\,76.902)\cdot10^{-6}$ |
| | 3 | 2115.10 | 1.67 | $(16.382 - i\,33.327)\cdot10^{-6}$ |
| | 4 | 3134.97 | 4.74 | $(168.391 - i\,191.999)\cdot10^{-6}$ |
| | 5 | 3991.89 | 0.91 | $(5.962 - I\,17.500)\cdot10^{-6}$ |

The machine tool was unable to handle larger depth of cuts due to chatter and its limited torque capacity. The chatter stability lobes of the cutter are predicted using time domain as well as frequency domain analytical methods. The time domain simulation considers the nonlinearities in the process, such as varying cutting constants along the insert, discontinuities along the flute due to inserts, and tool jumping out of cut due to excessive vibrations. The frequency domain analytical solution assumes constant average cutting constant and continuous cutting edges like in regular end mills. The stability lobes for half immersion down milling are predicted and experimentally verified with 0.050 mm/tooth feed rate (Figure 8). The presence of chatter is monitored the spectrum of sound signals measured using microphone placed close to the cutting zone. Although the analytical chatter stability assumes a simplified, linear process model, it is still able to predict the chatter stability lobes quite satisfactorily. The stability lobe generation in time domain took approximately two days of computer time and only few seconds in the frequency domain on a personal computer. The stability lobes indicated the presence of chatter at an axial depth of cut of 6.0 mm and spindle speed of 3150 rev/min. The measured and simulated values of surface finish and chatter vibration spectra are in good agreement. The chatter is caused by the first bending mode (473 Hz) of the spindle - cutter assembly. When the speed is increased to 5750 rev/min, the chatter disappeared as predicted by the stability lobe diagram and time domain simulations.

**Milling of $Ti_6Al_4V$ with Cutter II:** Titanium alloy $Ti_6Al_4V$ is milled using a Mitsubishi LER1606W20 R98244 cutter with two flutes and two different rectangular inserts (Mitsubishi CCMX083508ENA and ZCMX083508ERA HTi20T). There are three inserts placed on each flute. The cutter design model is formed as (Figure 9. ):

$$D_M = \begin{bmatrix} 3 & 3 & 3 & ; & 4 & 3 & 3 \\ 4.0 & 12.8 & 21.6 & ; & 5.0 & 16.5 & 25.3 \\ 8.7 & 8.7 & 8.7 & ; & 8.7 & 8.7 & 8.7 \\ 0.0 & 0.0 & 0.0 & ; & 0.0 & 0.0 & 0.0 \\ -10.0 & -10.0 & -10.0 & ; & -10.0 & -10.0 & -10.0 \\ 0.0 & 330.0 & 300.0 & ; & 180.0 & 150.0 & 120.0 \end{bmatrix} \quad (10)$$

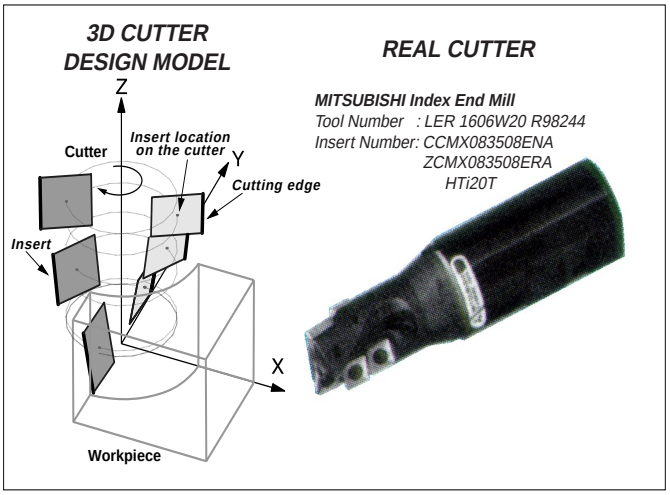


**Figure 9.** Mitsubishi inserted cutter Cutter II (Cutter number: LER1606W20 R98244; Insert numbers: CCMX083508ENA "insert dimensions; $a$=8.0 mm, $b$=8.0 mm" and ZCMX083508ERA "insert dimensions; $a$=8.0 mm, $b$=10.0 mm" HTi20T). See Eq. (10) for insert location parameters. Shank diameter=31.75 mm, Cutter diameter=25.4 mm, 2 flutes, 3 inserts on every flute.

The first raw indicates rectangular insert types 3 and 4. Both inserts have identical geometry except the cutting edge lengths. Insert 3 has edge dimensions ($a$=8.0 mm, $b$=8.0 mm), and the Insert 4 has ($a$=8.0 mm, $b$=10.0 mm). The Insert 4 is used as a wiper blade to smooth the cut surface. The cutting coefficients of the inserts are identified from slot milling tests conducted at different depths of cut (1.0 mm - 5.0 mm) and feed-rates (0.020-0.080 mm/tooth), and given in Table 3. The insert edge geometry does not change beyond the first 5.0 mm length, thus the cutting coefficients remain the same as the values at $z$=5.0 mm. The spindle speed was 500 rev/min. The cutting constants change as a function of insert's axial contact ($z$) with the material. The simulated and experimentally measured cutting forces for two sample cases are given in Figure 10. . The first case is slot milling with 5.0 mm axial depth of cut and 0.050 mm/tooth feed, and the second case is half immersion down milling with 16.0 mm axial depth of cut with 0.030 mm/tooth feed. The spindle speed was 500 rev/min. The measured and predicted cutting forces are in good agreement.

**Table 3.** The cutting coefficients for $Ti_6Al_4V$ with Cutter II ($0 \le z \le 5.0$ mm). Between 5.0 mm and 10.0 mm, the cutting coefficients are constant and the same as the values used at $z$=5.0 mm. The edge contact position ($z$) is expressed in millimeter.

| Cutting Coef. | Fitted curve | Correlation Coefficient |
|---|---|---|
| $K_{tc}$ [N/mm$^2$] | $81.8z^2 - 405.3z + 2562.1$ | 0.8232 |
| $K_{rc}$ [N/mm$^2$] | $110.7z^2 - 511.1z + 1862.3$ | 0.8931 |
| $K_{ac}$ [N/mm$^2$] | $-135.2z^2 + 935.8z - 1697.9$ | 0.8803 |
| $K_{te}$ [N/mm] | $-4.83z^2 + 17.50z + 25.80$ | 0.8260 |
| $K_{re}$ [N/mm] | $-5.84z^2 + 26.74z + 86.4$ | 0.9563 |
| $K_{ae}$ [N/mm] | $-4.83z^2 + 35.81z - 62.80$ | 0.9968 |

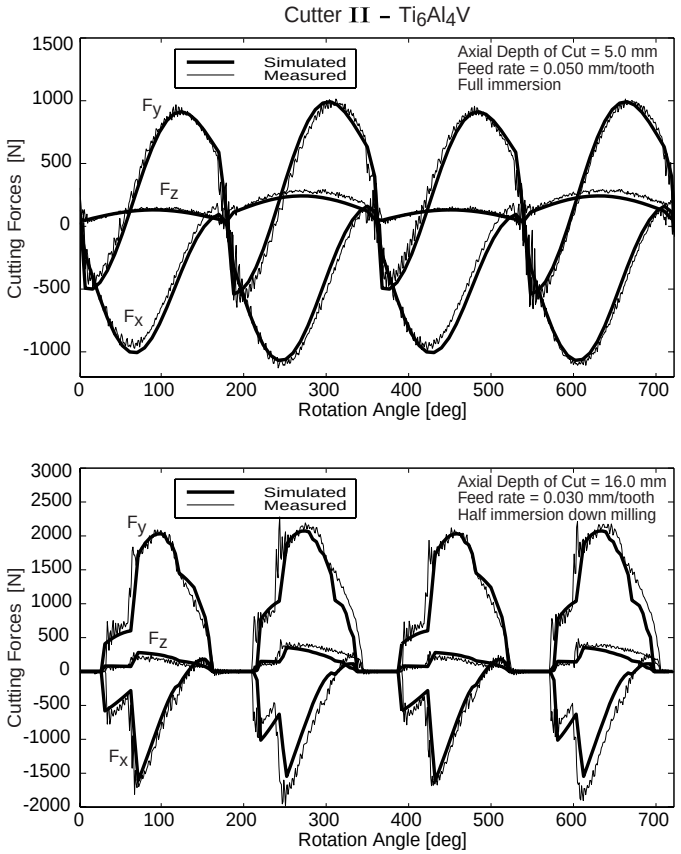


**Figure 10.** Measured and predicted cutting forces for $Ti_6Al_4V$ with Cutter II. Spindle speed is 500 rev/min. See Figure 9. for tool geometry and Table 3 for cutting coefficients.

## 5. CONCLUSION

A generalized mathematical model for inserted cutters has been developed. The model allows placing different inserts on the cutter body mathematically. Each insert is placed on the cutter body by defining its center from a cutter body coordinate system. The inserts can be oriented by rotating them about the three axis of the cutter body. The insert geometry is defined individually in a local coordinate system by its edge dimensions and shapes. By combining the vectorial representation of the insert center and cutting edge, the cutting edge of each insert is defined. The chip thickness, cutting force, chatter vibrations, dimensional surface finish and stability lobes of the milling process generated by the arbitrarily inserted cutters are evaluated. The proposed model allows the analysis of general indexed cutters, and it is experimentally proven using two industrial indexed cutters in milling of Al-7075 and $Ti_6Al_4V$ alloys.

## ACKNOWLEDGEMENTS

This research is supported NSERC, General Motors and Boeing under Cooperative Research and Development Research Grant.

## REFERENCES

Altintas, Y., and Budak, E., 1995, "Analytical Prediction of Stability Lobes in Milling", *Annals of CIRP*, Vol. 44(No.1), pp. 357-362.

Altintas, Y., and Lee, P., 1998, "Mechanics and Dynamics of Ball End Milling", *Transaction of ASME, Journal of Manufacturing Science and Engineering*, Vol. 120, pp. 684-692.

Altintas, Y., Montgomery, D., and Budak, E., 1992, "Dynamic Peripheral Milling of Flexible Structures", *Transactions of ASME Journal of Engineering for Industry*, Vol. 114, pp. 137-145.

Budak, E., Altintas, Y., and Armarego, E. J. A., 1996, "Prediction of Milling Force Coefficients From Orthogonal Cutting Data", *Transactions of ASME*, Vol. 118, pp. 216-224.

Ehmann, K. F., Kapoor, S. G., DeVor, R. E., and Lazoglu, I., 1997, "Machining Process Modeling: A Review", *Journal of Manufacturing Science and Engineering Transaction of the ASME*, Vol. 119(No.4-B), pp. 655-663.

Endres, W. J., DeVor, R. E., and Kapoor, S. G., 1995, "A Dual-Mechanism Approach to the Prediction of Machining Forces: Part I - Model Development: Part II - Calibration and Validation", *Transactions of ASME Journal of Engineering for Industry*, Vol. 117, pp. 526-541.

Engin, S., and Altintas, Y., 1999, "Generalized Modeling of Milling Mechanics and Dynamics: Part I – Helical End Mills".

Fu, H. J., Devor, R. E., and Kapoor, S. G., 1984, "A Mechanistic Model for the Prediction of the Force System in Face Milling Operation", *ASME Journal of Engineering for Industry*, Vol. 106(No.1), pp. 81-88.

Gu, F., Kapoor, S. G., Devor, R. E., and Bandyopadhyay, P., 1997, "An Enhanced Cutting Force Model for Face Milling With Variable cutter Feed Motion and Complex Workpiece Geometry", *Journal of Manufacturing Science and Engineering Transaction of the ASME*, Vol. 119(No.4), pp. 467-475.

Kim, H. S., and Ehmann, K. F., 1993, "A Cutting Force Model for Face Milling Operations", *International al Journal of Machine Tools and Manufacture*, Vol 33(5), pp. 651-673.

Martellotti, M.E., 1945, "An Analysis of the Milling Process. Part II: Down Milling", *Transactions of the ASME*, Vol. 67, pp. 233-251.

MillPro, 1998, "Milling Simulation Program", *University of British Columbia -Manufacturing Automation Laboratory*.

Montgomery, D., and Altintas, Y., 1991, "Mechanism of Cutting Force and Surface Generation in Dynamic Milling", *Transactions of ASME Journal of Engineering for Industry*, Vol. 113, pp. 160-168.

Spence, A., Altintas, Y., 1994, "A Solid Modeler Based Milling Process Simulation and Planning System", *Transactions of the ASME, Journal of Engineering for Industry*, Vol. 116, pp. 61-69.

Spiewak, S. A., 1994, "Analytical Modeling of Cutting Point Trajectories in Milling", *Transactions of the ASME, Journal of Engineering for Industry*, Vol. 116, pp. 440-448.

Wertheim, R., Satran, A., and Ber, A., 1994, "Modifications of the Cutting Edge Geometry and Chip Formation in Milling", *Annals of the CIRP*, Vol. 43(No. 1), pp. 63-68.